



Electron Localization Dynamics in the Triplet Excited State of $[\text{Ru}(\text{bpy})_3]^{2+}$ in Aqueous Solution

Marc-Etienne Moret,^[a, c] Ivano Tavernelli,^{*, [a]} Majed Chergui,^[b] and Ursula Rothlisberger^[a]

Abstract: Hybrid DFT/classical molecular dynamics of the long-lived triplet excited state of $[\text{Ru}(\text{bpy})_3]^{2+}$ (bpy = 2,2'-bipyridine) in aqueous solution is used to investigate the solvent-mediated electron localization and dynamics in the triplet metal-to-ligand charge-transfer (MLCT) state. Our studies reveal a solvent-induced breaking of the coordination symmetry with consequent localization of the photoexcited electron on one or two bipyridine units for the entire length of our simulation, which amounts to several picoseconds. Frequent electronic “hops” between the ligands constituting the pair are observed with a characteristic time of approximately half a picosecond.

Keywords: ab initio calculations • charge transfer • computer chemistry • molecular dynamics • photo-physics

Introduction

Charge separation is the physical phenomenon underlying virtually all schemes geared towards the conversion of light into chemical, electrical, and/or mechanical energy. Inorganic compounds have long been exploited in the study of photoinduced charge-transfer processes, for both fundamental

reasons^[1] and for applications such as solar-energy conversion.^[2] Understanding these processes would provide a basis for their manipulation, through synthetic or other means, to achieve control over charge separation and/or reactivity. By far the most frequently employed inorganic chromophores in this respect are the polypyridyl complexes of Group 8 metals, of which $[\text{Ru}(\text{bpy})_3]^{2+}$ (**1**, bpy = 2,2'-bipyridine) is the prototypical model system. Their extensive use, ranging from light harvesting in dendritic polymers^[1] to sensitization of wide band-gap semiconductors,^[2] testifies to the important role they play in molecular solar-energy research.


However, despite the enormous importance of the subject, the lack of knowledge about the localization and the dynamics of the photoexcited electron in the ligand system still constitute an embarrassing reality for the entire photochemistry and photophysics community. In fact, no experiment can provide a full picture of the photodynamics of the metal-to-ligand charge-transfer (MLCT) complexes and only partial, and sometimes contradictory, results are available.

The doorway state to charge separation in $[\text{Ru}(\text{bpy})_3]^{2+}$ is its lowest singlet excited state described as a metal-to-ligand charge-transfer (¹MLCT) state. Upon excitation it is known to undergo intersystem crossing to the long-lived (≈ 500 ns) ³MLCT state with unity quantum efficiency. The issue of delocalization and localization of the electron upon excitation has been debated in the literature of the past three decades. In the D_3 symmetry of the molecule, the transferred electron would have to be equally shared among the three bpy lig-

[a] M.-E. Moret, Dr. I. Tavernelli, Prof. U. Rothlisberger
Laboratoire de chimie et biochimie computationnelles
Ecole Polytechnique Fédérale de Lausanne
1015 Lausanne (Switzerland)
Fax: (41) 21-693-0320
E-mail: ivano.tavernelli@epfl.ch

[b] Prof. M. Chergui
Laboratoire de spectroscopie ultrarapide
Ecole Polytechnique Fédérale de Lausanne
1015 Lausanne (Switzerland)

[c] M.-E. Moret
Present address: Division of Chemistry and Chemical Engineering
California Institute of Technology
Pasadena, California 91125 (USA)

 Supporting information for this article is available on the WWW under <http://dx.doi.org/10.1002/chem.201000184>. It contains method validation and comparison with previous studies; details on the ground state and ³MLCT electronic structures and optimized geometries; time evolution of the molecular dipole (continuation) in the triplet state QM/MM simulation at 300 K (Figure S1) and 400 K (Figure S2); distribution of the C–C and C–N bond lengths of ligands 1, 2 and 3 computed from the triplet state QM/MM trajectory at 300 K (Figure S3).

ands.^[3,4] However, while it seems in general agreed that the electron localizes on one ligand, the question as to whether the electron starts off delocalized, and then localizes is still being discussed, just as the mechanism which leads to localization, for example, solvation dynamics and/or vibrational cooling. Femtosecond time-resolved absorption anisotropy measurements in different nitriles^[5] have been interpreted in terms of an initial delocalization of the electron over all three bpy ligands followed by solvent-driven localization on only one bpy on timescales of 60–170 fs, due to the inertial solvation dynamics occurring in response to the photo-induced charge transfer. However, the solvatochromism of [Ru(bpy)₃]²⁺^[6] and the Stark effect in electro-optical absorption^[7] suggest that the vertical excited state is already localized. A resonance Raman study^[8] suggested that symmetry breaking in the ground state of [Ru(bpy)₃]²⁺, possibly caused by complex formation with water molecules, is the cause for localization. Even when the electron is localized on a ligand, interligand electron transfer (so-called ILET) may occur in which the electron hops from a ligand to the next. Recently, time-resolved transient-absorption (TA) anisotropy measurements showed that the memory of the initially photoselected bipyridine ligand is lost within 1 ps,^[9] contradicting earlier reports that provided much longer timescales.^[10] However, this randomization process could take place in the early stages of photoexcitation (i.e., in the singlet excited state or before vibrational cooling), hence making the interpretation of these data in terms of interligand and electron dynamics in the thermalized, long-lived ³MLCT state questionable. The difficulty of TA lies on the fact that the MLCT states represent a manifold that undergoes internal conversion, intersystem crossing, and intramolecular vibrational relaxation, all of which may contribute to the scrambling of the initial polarization. In principle, polarization-dependent ultrafast fluorescence studies offer a more direct way of determining the depolarization of the system, but these are challenging because on the one hand the lifetime of the ¹MLCT is extremely short (≤ 30 fs^[11]), while on the other, the signal from the ³MLCT emission is too weak in the short time domain.^[11] Hybrid quantum-classical methods offer an alternative way of investigating the dynamics of electron localization. Here, we present quantum mechanics/molecular mechanics (QM/MM) simulations that explicitly include the effects of the solvent. What emerges from our study is that while localization occurs upon excitation, it is a dynamic process, as hops occur between ligands on timescales of 0.5–1 ps. Remarkably, localization occurs most often on two ligands (rather than only one) over the whole trajectory, with rare events for which delocalization is observed over all three ligands.

Computational Methods

DFT calculations: DFT calculations were performed using the Becke exchange functional,^[12] together with the Perdew contribution^[13] for correlation. The quality of this functional was tested against hybrid functional

calculations (Table SI.1 in the Supporting Information) showing that good accuracy can be achieved without including exact exchange. A plane wave (PW) basis set with a cutoff of 75 Ry was used. The core electrons were frozen and represented by Trouiller–Martins^[14] norm-conserving non-local pseudopotentials, in which scalar relativistic effects were included, but no spin-orbit coupling was taken into account. The one-electron wavefunctions were optimized by using the direct inversion of the iterative subspace (DIIS)^[15] algorithm with a wavefunction gradient threshold of 10^{-5} atomic units; when this algorithm did not converge, a preconditioned conjugate gradient (PCG)-based algorithm was used instead. DFT calculations were performed with the CPMD code,^[16] with the exception of those involving Pople-type basis sets, which were performed with Gaussian 03.^[17]

The first-principles molecular dynamics simulations were performed in the NVT ensemble using the Car–Parrinello Scheme^[18] with a time step of 4 a.u. (≈ 0.097 fs) and a fictitious electronic mass of 600 a.u. Constant temperature was assured by a Nosé–Hoover^[19,20] thermostat at 300 K with a coupling frequency of 2000 cm⁻¹.

QM/MM setup: We applied a QM/MM molecular dynamics technique based on Car–Parrinello molecular dynamics^[18] that has been demonstrated to be valid for the description of solvation properties of neutral as well as charged systems.^[21–28] The steric interaction between the QM and the MM part is modeled by a Lennard–Jones potential as described by the AMBER force-field, while the electrostatic interactions with the neighboring MM atoms are taken into account by the energy term given in Equation (1), in which q_i is the charge of MM atom i , \mathbf{r}_i is its position, $\rho(\mathbf{r}) = \rho^{\text{el}}(\mathbf{r}) + \rho^{\text{on}}(\mathbf{r})$ is the total (ionic and electronic) charge density of the quantum system, and $v(\mathbf{r})$ is a Coulomb potential modified at short range in order to avoid spurious overpolarization effects

$$E_{\text{el}} = \sum_i q_i \int d\mathbf{r} \rho(\mathbf{r}) v(|\mathbf{r} - \mathbf{r}_i|) \quad (1)$$

The electrostatic interaction between the QM system and the more distant MM atoms is modeled by coupling of the multipole moments of the quantum charge distribution with the classical point charges.^[21] These interaction potentials polarize the charge density of the QM system and thus affect its electronic properties. The QM subsystem (Ru complex) was treated at the DFT BP level as described above, while water and chloride were treated classically using the AMBER force field. The inherent periodicity in the plane wave calculations was circumvented solving Poisson’s equation for nonperiodic boundary conditions,^[29] while periodic boundary conditions were retained for the classical solvent cubic box of edge 45 Å. The electrostatic interaction between classical atoms is taken into account by the P3M method.^[30] The initial positions and momenta for the triplet state QM/MM simulations were obtained from an equilibrated ground state QM/MM trajectory.^[31]

Results and Discussion

The behavior of the lowest triplet state of **1** in aqueous solution was investigated by means of QM/MM simulations at 300 and 400 K. For comparison, a short Car–Parrinello simulation in the gas phase was also performed. The computed average triplet state energy of the [Ru(bpy)₃]²⁺ complex in water is about 2 eV (compared to the ground state), in good agreement with experiments.^[11] As a natural indicator for the localization of the unpaired electron, we use the electronic dipole moment of the complex, which is small when the electron is fully delocalized and becomes large when the electron is localized on one ligand. Thus, the dipole moment of the QM part was computed “on-the-fly” during all MD simulations. To remove the contribution to the dipole moment due to the rotation of the complex, we expressed

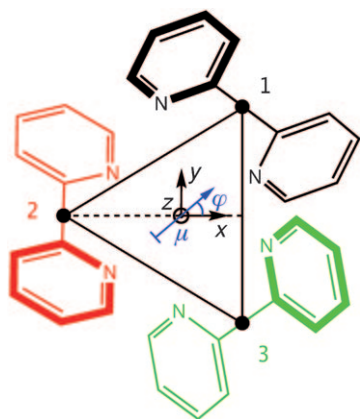


Figure 1. Internally defined coordinate system.

the electric dipole using an internal coordinate system defined in Figure 1. The equatorial plane is defined by the centers of the three C2–C2' bonds of the bpy ligands, with the origin at their barycenter and the coordinate axis oriented as shown in Figure 1. In the ideal D_3 -symmetrical geometry, the origin corresponds exactly to the Ru atom, and the \vec{z} axis to the C_3 axis of the complex. The dipole moment was then expressed in terms of spherical coordinates (μ, θ, ϕ) , for which μ is the magnitude, and θ and ϕ are the zenithal and azimuthal angles, respectively.

The time evolution of the dipole during the first 2 ps of QM/MM dynamics at 300 K is reported in Figure 2 (full trajectory in Figure S1 in the Supporting Information). The agreement between the intensity and the orientation of the dipole moment with the corresponding electronic structure is illustrated by means of a series of spin density plots computed for different structures sampled along the MD trajectory (Figure 2, bottom). As expected, the dipole moment strongly correlates with the localization of the spin densities: when the azimuthal angle ϕ is close to the vector pointing from the ruthenium ion to a specific ligand, the spin density at that ligand is high. Reciprocally, when this angle is close to π , the electron density is more equally shared among two ligands (ligands 1 and 3 according to our coordinates system—note that the dipole is oriented from the negative to the positive charge and therefore at $\phi=0$ the negative charge is localized along the positive x axis).

Strikingly, after about 300 fs, the unpaired electron mainly localizes on ligands 1 and 3, never visiting ligand 2 for the rest of the dynamics (≤ 5.1 ps). Since the trajectory is started directly on the $^3\text{MLCT}$ potential energy surface without the intermediacy of the $^1\text{MLCT}$ state (which is anyway very short lived, ≤ 30 fs^[11]), the observed relaxation time of approximately 300 fs can be seen as an estimate of the time needed for the water around the complex to adapt its structure after the $^3\text{MLCT}$ state is formed. This is especially true if we consider the peculiar solvation structure of $[\text{Ru}(\text{bpy})_3]^{2+}$ made of a chain-like hydrogen bonded sequence of water molecules in the interligand space (Figure 3), which was also observed in the ground-state dynamics.^[31]

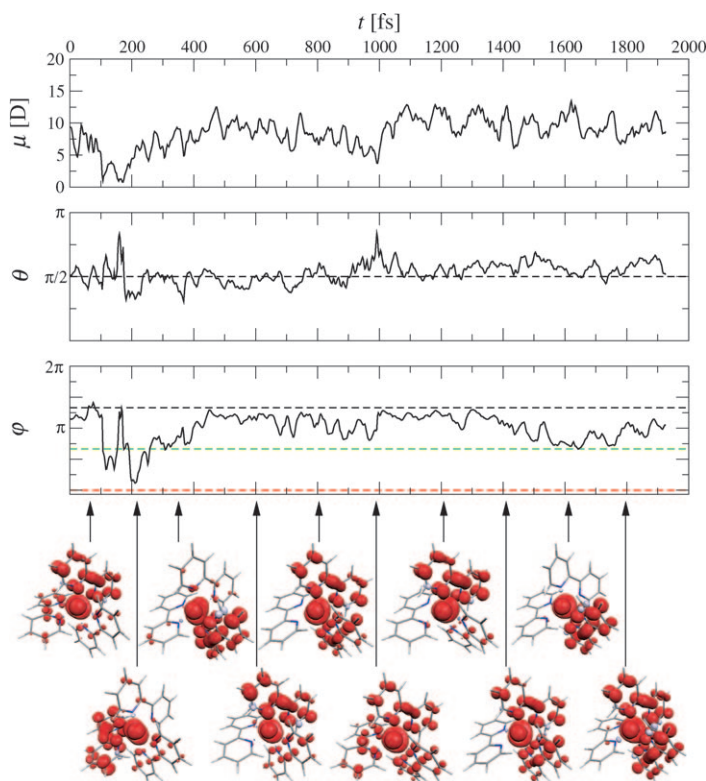


Figure 2. Top: Time evolution of the dipole (in Debyes) in spherical coordinates during the triplet state QM/MM simulation at 300 K. The dashed lines at ϕ angles of 0, $2\pi/3$, $4\pi/3$ represent the direction of vectors pointing from the center of ligands 1, 2, and 3, respectively, to the ruthenium atom. They correspond to the localization of the unpaired electron on ligand 2 (red), 3 (green), 1 (black), respectively. Bottom: spin densities computed from snapshots from the QM/MM trajectory.

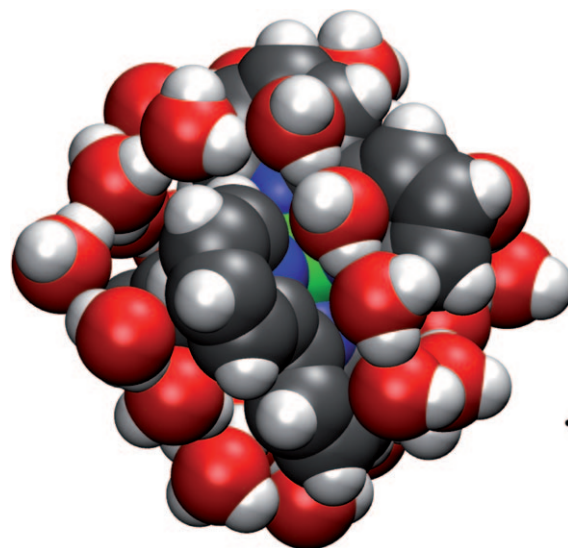


Figure 3. Snapshot from the QM/MM simulation in the triplet state, showing the structure of the first water shell. The atoms are represented by spheres of standard van der Waals radii, with the following color code: white, H; red, O; gray, C; blue, N; green, Ru. The image represents all atoms in a radius of seven Ångströms from the ruthenium with the exception a few hydrogen atoms from the second shell that have been removed for clarity.

The distribution of the dipole-moment orientation summed over the whole simulation time is plotted in Figure 4 (black line). The average value (8.6 D) of the

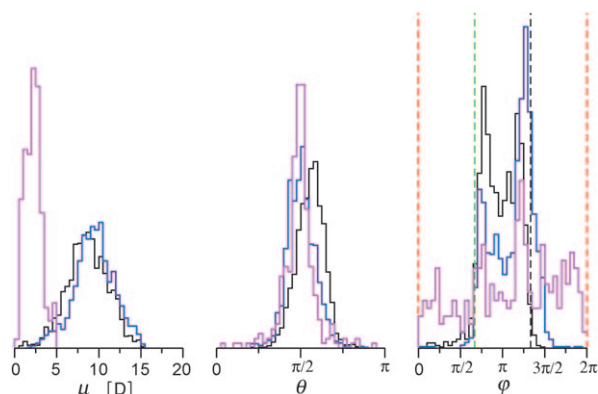


Figure 4. Distribution of the dipole spherical coordinates computed from QM/MM simulations of the first triplet state of $[\text{Ru}(\text{bpy})_3]^{2+}$ in water at 300 K (black) and 400 K (blue), and from a CP simulation in the gas phase (magenta).

dipole for the MLCT state (left panel) is in very good agreement with the experimental value reported in reference [7], in which a dipole change of ≈ 8.3 D with respect to the ground state ($\mu = 0$ D) was measured after correcting for the local field. The distribution of the azimuthal angle ϕ is bimodal, indicating that the unpaired electron is generally located either on ligand 1 or on ligand 3, but intermediate situations in which the unpaired electron is delocalized on both ligands also have a significant contribution. The fact that the spin density is never significantly located on one of the ligands (here ligand 2) for several picoseconds seems at first inconsistent with the experimental observation that the $^3\text{MLCT}$ state is randomized after at most 1 ps.^[9] However, depolarization can also come about even if one of the ligands is never visited, since the hops of typically 0.5 ps in Figure 2 can lead to quite significant reorientations of the dipole. We cannot excluded that the fate of the system is decided at very early times, as the $^1\text{MLCT}$ state has a lifetime of ≤ 30 fs, and appears vibrationally cold (at least if one considers the Franck–Condon modes).^[11] Our results seem in accord with the reported vibrational cooling time of 3–5 ps in the $^3\text{MLCT}$ state^[32] and call therefore for a reexamination of the depolarization dynamics.

In an attempt to observe a transition to a different state in which the unpaired electron would also be partially distributed on the so far never visited ligand 2 (ϕ close to 0), a 4 ps long QM/MM MD simulation at a temperature of 400 K was performed. The desired transition was not observed during this time, but the dipole moment distribution (Figure 4, blue line) shows that the unpaired electron tends to be even more sharply localized than at 300 K: the maxima of the ϕ distribution get closer to the ideal values of $2\pi/3$ and $4\pi/3$, and the central region around $\phi = \pi$ is depleted. A closer inspection of the corresponding time series

(Figure S2 in the Supporting Information) shows that the unpaired electron seems to oscillate between ligands 1 and 3, residing on each for a period of 1–2 ps if one considers the angular distribution in Figure 2 (although localization is not so clear-cut if one looks at the spin densities). This period is longer than the characteristic time for the solvent-dipole reorientation in the bulk, and we attribute this effect to slower solvent reorganization motions of the water molecules intercalated in the ligands.^[31] From the QM/MM trajectory at 300 K, the calculation of the electrostatic potential distributions induced by all solvent molecules at the midpoint of the C2–C2' bonds reveals a clear difference among the three ligands. In fact, the distribution for ligand 2 (the one that never carries the unpaired electron) is clearly shifted by about 0.5–0.8 V compared to the one of the other two ligands (Figure 5). This implies that the reorganization

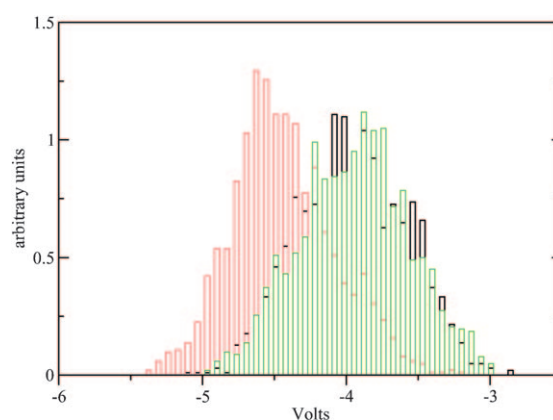


Figure 5. Distribution functions of the electrostatic potential generated by all solvent molecules at the midpoint of the C2–C2' bonds of the three ligands. Black, ligand 1; red, ligand 2; green, ligand 3.

energy required for the transfer of the excess electron in the ligand system from one or both ligands bearing the extra charge to the neutral one has an energy cost of the order of 1 eV. Unfortunately, the computationally affordable time window of our simulations is too narrow to allow a more accurate characterization of these solvent effects.

The critical role of solvation in the localization of the unpaired electron was confirmed by a DFT-based MD simulation performed in the first triplet state of $[\text{Ru}(\text{bpy})_3]^{2+}$ at 300 K in vacuum. Under these conditions, the dipole moment is on average three times smaller than in water (Figure 4, magenta line), and its projection on the equatorial plane is evenly distributed towards all directions (Figure 6). Thus, in the gas phase, the first triplet state of $[\text{Ru}(\text{bpy})_3]^{2+}$ is best described as a delocalized state with fast fluctuations, while the solvent is needed for localization.

A close inspection of the time evolution of the dipole moment in solution reveals the occurrence of several short periods in which it becomes small (< 5 D) and gets far off the equatorial plane, indicating a strong delocalization of the unpaired electron (for example, around $t = 993$ fs in the

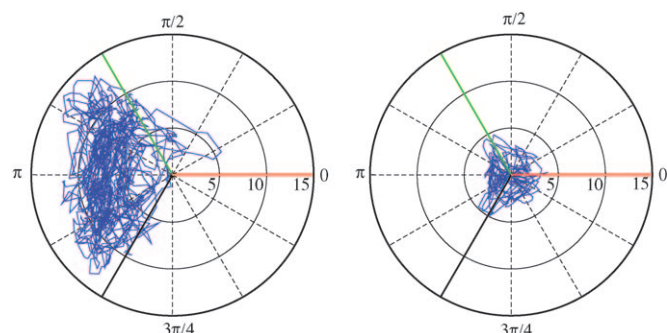


Figure 6. Projection of the dipole moment (in Debyes) onto the equatorial plane (see Figure 1). Left: in water at 300 K; Right: in gas phase. The directions corresponding to ligands 1, 2, and 3 are indicated in black, red and green respectively.

300 K trajectory, and around $t=1018$ fs at 400 K). One could expect that from a delocalized state the probability for the electron to relocalize on each of the three ligands would be equal, but this was found not to be the case: the electron always comes back to ligands 1 or 3.

A more detailed picture of one of these events was obtained by re-computing the part of the 400 K trajectory in the interval $990 < t < 1140$ fs and sampling the Car–Parrinello spin density. A plot of the spin densities integrated on each ligand and on the metal center as a function of time is shown in Figure 7. The spin density on the ruthenium center

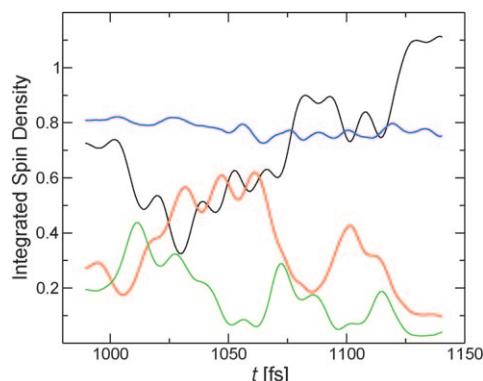


Figure 7. Integrated spin density on the ruthenium atom (blue) and on each ligand (ligand 1: black, ligand 2: red, ligand 3: green) during a “missed jump” event in the 400 K trajectory.

stays constant during the considered time interval, showing that unoccupied d orbitals are not involved. At the beginning of this time interval, the unpaired electron is predominantly localized on ligand 1. When the dipole magnitude reaches its minimum ($t=1018$ fs), the spin density is almost equally distributed over all three ligands. The electron is then delocalized over ligands 1 and 2 for about 50 fs and then finally comes back to its initial location on ligand 1. This is likely due to the inertia of the solvent shell, which keeps the memory of the position of the electron and brings it back to its initial position.

The geometrical consequences of the solvent-induced electron localization were studied by means of a statistical analysis of key bond lengths (Table 1 and Figure S3). The

Table 1. Mean values (standard deviation) for selected bond lengths from the triplet QM/MM trajectory and the corresponding values from the 3 MLCT and ground-state (GS) geometries optimized at 0 K.

| Bond | Ligand 1 | Ligand 2 | Ligand 3 | 3 MLCT | GS ^[31] |
|--------|-----------|-----------|-----------|-----------|--------------------|
| N–C2 | 1.392(17) | 1.377(17) | 1.390(19) | 1.384 | 1.373 |
| C2–C3 | 1.413(13) | 1.402(14) | 1.412(16) | 1.407 | 1.400 |
| C3–C4 | 1.384(12) | 1.392(10) | 1.387(10) | 1.385 | 1.391 |
| C4–C5 | 1.412(15) | 1.402(12) | 1.411(13) | 1.406 | 1.396 |
| C5–C6 | 1.387(11) | 1.390(11) | 1.387(12) | 1.385 | 1.389 |
| C6–N | 1.358(11) | 1.354(12) | 1.357(12) | 1.357 | 1.355 |
| C2–C2' | 1.441(22) | 1.459(19) | 1.445(20) | 1.449 | 1.470 |
| Ru–N | 2.081(45) | 2.071(39) | 2.091(42) | 2.074 | 2.075 |

average Ru–N length is slightly longer than the one obtained from the gas-phase-optimized geometry: 2.08 versus 2.07 Å. The slight lengthening of this bond may be due to solvation or to the anharmonicity of the corresponding vibrational modes. However, the differences in the Ru–N bond length for individual ligands are rather small compared to the corresponding standard deviation (ca. 0.01 vs. ca. 0.04 Å) and uncorrelated with the location of the unpaired electron. Comparison with the singlet ground state reveals no clear difference in the Ru–N bond length, but this is not surprising since the experimentally determined bond shortening of 0.03 Å^[33] is smaller than the thermal fluctuations of the corresponding bond-length distributions obtained from the DFT calculations at 300 K (Table 1).

While we could observe no significant differentiation in the coordination geometry, the intraligand bonds were found to be affected by the localization of the spin density. The distributions of these bond lengths (Table 1) are virtually identical for ligands 1 and 3 (which share the unpaired electron), and, as expected, different for ligand 2, which is never visited. The most sensitive bonds are the N–C2, C2–C3, C4–C5 bonds, which are about 0.01 Å longer for ligands 1 and 3, and the C2–C2' bond, which is about 0.01 to 0.02 Å shorter for ligands 1 and 3. As expected, the values for the triplet-state-optimized geometry, for which the unpaired electron is delocalized over all three ligands, lie between the values for the ligands bearing the unpaired electron and those for the one without. These observations are consistent with the shape of the LUMO of the ligand (Supporting Information), which is bonding with respect to the C2–C2' bond, and antibonding with respect to the three other bonds.

Conclusion

In summary, the MLCT state of tris(bipyridine)ruthenium(II) in aqueous solution has been investigated by means of Car–Parrinello QM/MM simulations. In the gas phase, the unpaired electron is found to be delocalized over the

three bipyridine ligands. In contrast, in solution the excited electron is most of the time located on a subset of ligands confirming the conclusions from excited-state Raman data^[3,4] and, more importantly, from Stark spectroscopy.^[7] However, contrary to the generally accepted idea of localization on a single ligand, our results show a dynamic process in which localization is either on two ligands or one ligand with frequent hops between these two regimes. Furthermore, and as a consequence, our calculations do not support a simple interligand electron-transfer (ILET) mechanism involving well-localized ligand orbitals, but suggest a different process in which thermal relaxation of the complex and of the surrounding solvent shell breaks the coordination symmetry and drives spin-density localization on mainly two ligands, and occasionally on only one. The low-energy-barrier, spin-density fluctuations among the ligands constituting this pair have been characterized in detail and show a period of about 0.5–1 ps. On some rarer occasions, the electron is delocalized over all three ligands for very short periods of time, but it then comes back to one or both preferred ligands, which show a more favorable solvation structure. This behavior most likely arises from relatively slow solvent dynamics, which is related to the peculiar structure of the immediate solvation shells.^[31] In fact, electron-transfer events between different pairs of ligands require larger structural reorganizations of the solvent with an energy cost that can be quantified to be of the order of 0.5–0.8 eV, and therefore cannot be observed in our simulations.

Acknowledgements

Prof. A. Vlcek is acknowledged for interesting discussions.

- [1] V. Balzani, A. Juris, M. Venturi, S. Campagna, S. Serroni, *Chem. Rev.* **1996**, 96, 759–834.
- [2] K. Kalyanasundaram, M. Grätzel, *Coord. Chem. Rev.* **1998**, 177, 347–414.
- [3] A. Juris, V. Balzani, F. Barigelli, S. Campagna, P. Belser, A. Von Zelewsky, *Coord. Chem. Rev.* **1988**, 84, 85–277.
- [4] K. D. Demadis, C. M. Hartshorn, T. J. Meyer, *Chem. Rev.* **2001**, 101, 2655–2686.
- [5] A. T. Yeh, C. V. Shank, J. K. McCusker, *Science* **2000**, 289, 935–938.
- [6] E. M. Kober, P. Sullivan, T. J. Meyer, *Inorg. Chem.* **1984**, 23, 2098–2104.
- [7] D. Oh, S. Boxer, *J. Am. Chem. Soc.* **1989**, 111, 1130–1131.
- [8] M. A. Webb, J. Fritz, J. L. McHale, *J. Raman Spectrosc.* **2001**, 32, 481–485.
- [9] S. Wallin, J. Davidsson, J. Modin, L. Hammarstrom, *J. Phys. Chem. A* **2005**, 109, 4697–4704.
- [10] R. Malone, D. J. Kelly, *J. Chem. Phys.* **1991**, 95, 8970.
- [11] A. Cannizzo, F. van Mourik, W. Gawelda, G. Zgrablic, C. Bressler, M. Chergui, *Angew. Chem.* **2006**, 118, 3246–3248; *Angew. Chem. Int. Ed.* **2006**, 45, 3174–3176.
- [12] A. D. Becke, *Phys. Rev. A* **1988**, 38, 3098–3100.
- [13] J. P. Perdew, *Phys. Rev. B* **1986**, 33, 8822–8824.
- [14] N. Troullier, J. L. Martins, *Phys. Rev. B* **1991**, 43, 1993–2006.
- [15] J. Hutter, H. P. Lüthi, M. Parrinello, *Comput. Mater. Sci.* **1994**, 2, 244–248.
- [16] CPMD, IBM Corp **1990–2004**, MPI für Festkörperforschung Stuttgart **1997–2001**.
- [17] Gaussian 03 (Revision B.03), M. J. Frisch, G. W. Trucks, H. B. Schlegel, G. E. Scuseria, M. A. Robb, J. R. Cheeseman, J. A. Montgomery Jr., T. Vreven, K. N. Kudin, J. C. Burant, J. M. Millam, S. S. Iyengar, J. Tomasi, V. Barone, B. Mennucci, M. Cossi, G. Scalmani, N. Rega, G. A. Petersson, H. Nakatsuji, M. Hada, M. Ehara, K. Toyota, R. Fukuda, J. Hasegawa, M. Ishida, T. Nakajima, Y. Honda, O. Kitao, H. Nakai, M. Klene, X. Li, J. E. Knox, H. P. Hratchian, J. B. Cross, C. Adamo, J. Jaramillo, R. Gomperts, R. E. Stratmann, O. Yazyev, A. J. Austin, R. Cammi, C. Pomelli, J. W. Ochterski, P. Y. Ayala, K. Morokuma, G. A. Voth, P. Salvador, J. J. Dannenberg, V. G. Zakrzewski, S. Dapprich, A. D. Daniels, M. C. Strain, O. Farkas, D. K. Malick, A. D. Rabuck, K. Raghavachari, J. B. Foresman, J. V. Ortiz, Q. Cui, A. G. Baboul, S. Clifford, J. Cioslowski, B. B. Stefanov, G. Liu, A. Liashenko, P. Piskorz, I. Komaromi, R. L. Martin, D. J. Fox, T. Keith, M. A. Al-Laham, C. Y. Peng, A. Nanayakkara, M. Challacombe, P. M. W. Gill, B. Johnson, W. Chen, M. W. Wong, C. Gonzalez, J. A. Pople, Gaussian, Inc., Pittsburgh, PA, **2004**.
- [18] R. Car, M. Parrinello, *Phys. Rev. Lett.* **1985**, 55, 2471–2474.
- [19] S. Nosé, *Mol. Phys.* **1984**, 52, 255–268.
- [20] W. G. Hoover, *Phys. Rev. A* **1985**, 31, 1695–1697.
- [21] A. Laio, J. Van de Vondele, U. Rothlisberger, *J. Chem. Phys.* **2002**, 116, 6941–6947.
- [22] U. F. Röhrig, F. Irmgard, J. Hutter, A. Laio, J. VandeVondele, U. Rothlisberger, *ChemPhysChem* **2003**, 4, 1177–1182.
- [23] C. Gossens, I. Tavernelli, U. Rothlisberger, *CHIMIA* **2005**, 59, 81–84.
- [24] M. E. Moret, E. Tapavicza, L. Guidoni, U. Röhrig, M. Sulpizi, I. Tavernelli, U. Rothlisberger, *CHIMIA* **2005**, 59, 493–498.
- [25] M. Cascella, M. Cuendet, I. Tavernelli, U. Rothlisberger, *J. Phys. Chem. B* **2007**, 111, 10248–10252.
- [26] M. Cascella, A. Magistrato, I. Tavernelli, P. Carloni, U. Rothlisberger, *Proc. Natl. Acad. Sci. USA* **2006**, 103, 19641–19646.
- [27] S. Komin, C. Gossens, I. Tavernelli, U. Rothlisberger, D. Sebastiani, *J. Phys. Chem. B* **2007**, 111, 5225–5232.
- [28] C. Gossens, I. Tavernelli, U. Rothlisberger, *J. Am. Chem. Soc.* **2008**, 130, 10921–10928.
- [29] G. J. Martyna, M. E. Tuckerman, *J. Chem. Phys.* **1999**, 110, 2810–2821.
- [30] B. A. Luty, W. F. van Gunsteren, *J. Chem. Phys.* **1996**, 104–105, 2581–2587.
- [31] M. E. Moret, I. Tavernelli, U. Rothlisberger, *J. Phys. Chem. B* **2009**, 113, 7737–7744.
- [32] A. N. Tarnovsky, W. Gawelda, M. Johnson, C. Bressler, M. Chergui, *J. Phys. Chem. B* **2006**, 110, 26497–26505.
- [33] W. Gawelda, M. Johnson, F. M. F. de Groot, R. Abela, C. Bressler, M. Chergui, *J. Am. Chem. Soc.* **2006**, 128, 5001–5009.

Received: January 23, 2010

Published online: April 29, 2010